Higher-resolution tropopause folding accounts for more stratospheric ozone intrusions

Samuel Bartusek[1], Yutian Wu[2], Mingfang Ting[1], Cheng Zheng[3], Arlene Fiore[4], Michael Sprenger[5], and Johannes Flemming[6]

[1]Columbia University
[2]Lamont-Doherty Earth Observatory of Columbia University
[3]Lamont-Doherty Earth Observatory, Columbia University
[4]MIT
[5]Institute for Atmospheric and Climate Science
[6]ECMWF

November 22, 2022

Abstract

Ozone in the troposphere is a pollutant and greenhouse gas, and it is crucial to better understand its transport from the ozone-rich stratosphere. Tropopause folding, wherein stratospheric air intrudes downward into the troposphere, enables stratosphere-to-troposphere ozone transport (STT). However, systematic analysis of the relationship between folding and tropospheric ozone, using data that can both capture folding's spatial scales and accurately represent tropospheric chemistry, is lacking. Here, we compare folding in both high-resolution (0.25°) reanalysis ERA5 and low-resolution (0.75°) chemical reanalysis CAMSRA over one year. High-resolution folding is dramatically more frequent and significantly better-correlated with tropospheric ozone. In particular, folding of deep tropospheric extent is nearly 100% missing at low resolution, and folding–ozone correlations increase most with resolution along midlatitude storm tracks, where deep folding is most common. Our results imply that STT is more attributable to tropopause folding than implied by low-resolution analysis, likely associated with resolving filamentary, deep folding.

Higher-resolution tropopause folding accounts for more stratospheric ozone intrusions

Samuel Bartusek[1,2], Yutian Wu[1], Mingfang Ting[1,2], Cheng Zheng[1], Arlene Fiore[3], Michael Sprenger[4], Johannes Flemming[5]

[1]Lamont-Doherty Earth Observatory, Columbia University, Palisades, NY, USA
[2]Department of Earth and Environmental Sciences, Columbia University, New York, NY, USA
[3]Department of Earth, Atmospheric, and Planetary Sciences, Massachusetts Institute of Technology, Cambridge, MA, USA
[4]Institute for Atmosphere and Climate Science, ETH Zürich, Zürich, Switzerland
[5]European Centre for Medium-Range Weather Forecasts (ECMWF), Reading, UK

Key Points:

- Tropopause folding is significantly more frequent with increasing atmospheric grid-cell resolution.
- Nearly 90% of folding in ERA5 (nearly 100% of Deep folding) is unrepresented at the resolution of ERA-Interim.
- High-resolution folding is more strongly correlated with tropospheric ozone, driven by deeper and more filamentary folding.

Corresponding author: Samuel Bartusek, `samuel.bartusek@columbia.edu`

Abstract

Ozone in the troposphere is a pollutant and greenhouse gas, and it is crucial to better understand its transport from the ozone-rich stratosphere. Tropopause folding, wherein stratospheric air intrudes downward into the troposphere, enables stratosphere-to-troposphere ozone transport (STT). However, systematic analysis of the relationship between folding and tropospheric ozone, using data that can both capture folding's spatial scales and accurately represent tropospheric chemistry, is lacking. Here, we compare folding in both high-resolution (0.25°) reanalysis ERA5 and low-resolution (0.75°) chemical reanalysis CAMSRA over one year. High-resolution folding is dramatically more frequent and significantly better-correlated with tropospheric ozone. In particular, folding of deep tropospheric extent is nearly 100% missing at low resolution, and folding–ozone correlations increase most with resolution along midlatitude storm tracks, where deep folding is most common. Our results imply that STT is more attributable to tropopause folding than implied by low-resolution analysis, likely associated with resolving filamentary, deep folding.

Plain Language Summary

"Tropopause folding" refers to high-altitude atmospheric events wherein the "tropopause" (the boundary separating the troposphere, the lowest atmospheric layer, from the stratosphere above it) is perturbed, "folding" downward and allowing stratospheric air to intrude into the troposphere. These intrusions can enable stratosphere-to-troposphere transport (STT) of ozone, a pollutant and greenhouse gas in the troposphere—however, how strongly such events affect tropospheric ozone remains unclear. Here, we identify tropopause folding occurrences in both high- and low-resolution representations of atmospheric motion throughout one year, and assess how strongly each representation of folding is related to the estimated movement of tropospheric ozone. First, a high-resolution view reveals that folding events are much more frequent and widespread—and penetrate further into the troposphere, becoming more filamented—than visible at lower resolution. Moreover, folding at higher resolution is more closely correlated with tropospheric ozone behavior. These findings imply that folding may exert influence over a larger proportion of ozone STT (and potentially of the overall behavior of tropospheric ozone) than is suggested by coarse representations of folding. Furthermore, they underscore the importance of representing such skinny, filamentary features in estimates of atmospheric motion and transport of gases.

1 Introduction

Ozone in the stratosphere is beneficial to life on earth, but in the troposphere (where it is much rarer) it is a pollutant hazardous to human health and crops (Krzyzanowski & Cohen, 2008; Monks et al., 2015) and an effective greenhouse gas (Myhre et al., 2013). Understanding the sources of tropospheric ozone is thus societally and climatically important. While photochemical production is the largest source of tropospheric ozone, stratosphere-to-troposphere transport (STT) is a significant contributor (Neu et al., 2014; Hess et al., 2015; Williams et al., 2019), and stratospheric influence on tropospheric ozone is projected to strengthen due both to global-warming-related changes in the stratospheric circulation and to stratospheric ozone recovery (Hegglin & Shepherd, 2009; Hess et al., 2015; Banerjee et al., 2016; Meul et al., 2018; Akritidis et al., 2019; Fu & Tian, 2019).

The dominant mechanism for STT of air is tropopause folding (Stohl et al., 2003), wherein an intrusion of the stratosphere into the troposphere allows exchange between the two layers, increasing local upper- and mid-tropospheric ozone concentrations (Danielsen, 1968; Shapiro, 1980). Folding is responsible for large stratospheric influence on surface ozone and air-quality-exceedance events in some regions—notably the summertime eastern Mediterranean, Middle East, and Afghanistan (Tyrlis et al., 2014; Zanis et al., 2014; Akritidis et al., 2016) and the wintertime and springtime western United States (Langford et al., 1996; Langford & Reid, 1998; Langford et al., 2009; Lefohn et al., 2012; Lin et al., 2012; Skerlak et al., 2014; Lin et al., 2015; Wang et al., 2020) and Tibetan Plateau (Sprenger et al., 2003; X. L. Chen et al., 2011; X. Chen et al., 2013; Skerlak et al., 2014). However, this influence is not well constrained, and it is important to more systematically understand tropopause folding's role in influencing ozone STT and tropospheric ozone (Beekmann et al., 1997; Skerlak et al., 2014).

Gaps in understanding the relationships between tropopause folding, ozone STT, and tropospheric ozone have persisted for decades, limited by both meteorological and chemical data. While global-scale studies have analyzed folding itself (Skerlak et al., 2015; Akritidis et al., 2021) and its role in STT (Sprenger et al., 2003; Akritidis et al., 2019), to date such analysis has been restricted to low horizontal resolution (>80 km, e.g., ERA-

Interim). However, because folding is a meso- to synoptic-scale process, capturing fold morphology and fold-related turbulent STT processes requires resolutions <50 km (Knowland et al., 2017; Buker et al., 2005; Spreitzer et al., 2019). Consequently, the frequency of "double-tropopause" structures (of which folding is one type) is significantly higher in high-resolution ERA5 versus ERA-Interim (Hoffmann & Spang, 2022). High-resolution observational evidence, although sparse and localized, has suggested that atmospheric transport structures are horizontally and vertically filamentary, characterized by thin, diffusion-resistant layers (Danielsen, 1959; Appenzeller & Davies, 1992; Appenzeller et al., 1996; Newell et al., 1996, 1999; Trickl et al., 2010, 2020). Resolution may therefore greatly impact the representation of tropopause folding and its associated transport. Second, the fidelity of reanalysis ozone (particularly tropospheric) is constrained by both observational sparseness and, crucially, a lack of integrated chemical transport models (Dragani, 2010; Knowland et al., 2017; Wargan et al., 2017; Park et al., 2020). Therefore, despite reanalysis- and observation-based research on folding and its STT and ozone impacts (largely separately), a systematic global-scale relation of tropospheric ozone to tropopause folding has remained elusive.

Characterization of tropopause folding and its relationship with tropospheric ozone therefore lacks both (1) analysis of folding in a global dataset of sufficient meteorological fidelity, and (2) analysis of its ozone impacts in a global dataset of sufficient chemical fidelity. Here, addressing both gaps, we identify folding throughout one year in both high-resolution reanalysis ERA5 and a lower-resolution chemical reanalysis CAMSRA (with meteorology assimilated nearly-identically to ERA5 but at the resolution of ERA-Interim), and assess the relationship between both folding datasets and tropospheric ozone (derived from CAMSRA). Specifically, we address the following questions:

1. How are frequencies and global distributions of folding affected by spatial resolution?
2. How is the relationship between folding and tropospheric ozone affected by folding resolution?
3. How may folding frequency or morphology differences account for differing folding–ozone relationships?
4. What do our findings imply about ozone STT associated with folding, and tropospheric transport structures generally?

2 Data and Methods

We analyze data throughout 2012 from reanalyses CAMSRA (Copernicus Atmosphere Monitoring Service Reanalysis; European Center for Medium-range Weather Forecasting [ECMWF]) and ERA5 (ECMWF Reanalysis v5). CAMSRA (Inness et al., 2019) is a new chemical reanalysis at T255 spectral horizontal resolution (0.75°, 79 km grid) and 60 vertical levels to 0.1 hPa. ERA5 (Hersbach et al., 2020) is the latest ECMWF meteorological reanalysis at T639 resolution (0.25°, 31 km) and 137 levels to 0.01 hPa. Both reanalyses are produced by ECMWF's Integrated Forecasting System (IFS) using 4D-Var data assimilation; ERA5 uses IFS Cycle 41r2 and CAMSRA uses Cycle 42r1 (both implemented in 2016). CAMSRA meteorological fields are at the resolution of ERA-Interim (Dee et al., 2011) but produced with an updated model cycle nearly equivalent to that of ERA5 (ERA-Interim used Cycle 31r2, implemented in 2006)—therefore, the difference between CAMSRA and ERA5 meteorology is likely almost entirely due to resolution, even more strictly than between ERA-Interim and ERA5. From each reanalysis, we obtained six-hourly zonal and meridional wind components, potential temperature, and specific humidity at model levels up to 50 hPa, and surface pressure.

From CAMSRA, we also obtained ozone at pressure levels 250 hPa, 500 hPa, and 850 hPa, and a stratospheric ozone tracer (O_3S) interpolated to the same pressure levels from model levels. Unlike other reanalyses that assimilate ozone observations (such as NASA's Modern-Era Retrospective Analysis for Research and Applications 2 [MERRA-2], and ERA5), CAMSRA employs a chemical transport model (CTM) integrated into IFS—the Carbon Bond 2005 (CB05) chemistry mechanism, derived from Transport Model 5 (Huijnen et al., 2010; Flemming et al., 2015). While two previous chemistry reanalyses from ECMWF (MACC and GEMS) also employed a CTM, it remained two-way coupled to IFS instead of directly integrated (on-line) within it, and while one other reanalysis employs a CTM (Tropospheric Chemical Reanalysis 2 [TCR-2] from the Japan Agency for Marine-Earth Science and Technology [JAMSTEC]) it is of much coarser resolution (1.1°, 27 levels). A regional study found the inclusion of a dedicated CTM in reanalyses, as opposed to a one-way meteorology-chemistry relationship, to be more determinative of tropospheric composition fidelity than other factors such as resolution (Park et al., 2020). Furthermore, CAMSRA ozone has been shown to be broadly consistent with observations in the upper troposphere during stratospheric intrusions over Europe, despite overestimation in some sites (Akritidis et al., 2022). Stratospheric ozone in CAM-

SRA is parameterized using the Cariolle scheme (Cariolle & Déqué, 1986; Cariolle & Teyssèdre, 2007), and subject to data assimilation. O_3S is identical to total ozone in the stratosphere, but once across the tropopause (a spatially-varying pressure threshold fixed in time) it is freely transported and subject to chemical loss and deposition, but not production. It therefore roughly represents the portion of tropospheric ozone deriving from the stratosphere, likely tending towards an upper limit.

To identify tropopause folding in CAMSRA and ERA5, we apply a modified version of the algorithm of Skerlak et al. (2015) (building on Sprenger et al., 2003; Skerlak et al., 2014). The algorithm first defines the dynamical tropopause as the lower of the ±2 Potential Vorticity Unit (PVU) or 380 K potential temperature surface. At each timestep, folding is identified in each atmospheric column in which the tropopause is crossed in the vertical three or more times. Pressure values of the three crossings (interpolated between model levels based on the PV profile) are saved: $pmin$ and $pmax$ are the pressures of the upper and lower crossings and dp is the pressure difference between the upper and middle crossings (Figure 1a). Folded columns are classified into three depth ranges: Shallow (50 hPa $\leq dp <$ 200 hPa), Medium (200 hPa $\leq dp <$ 350 hPa), and Deep ($dp \geq$ 350 hPa), ignoring folding < 50 hPa. However, high-PV anomalies can arise in the troposphere independently from folding (e.g., fully cut-off from the stratosphere, or generated by diabatic or surface frictional processes). Therefore, to avoid spuriously identifying folding, the algorithm labels each 3D grid cell as either troposphere, stratosphere, troposphere but high-PV, or stratosphere but low-PV. In our analysis, ERA5's high resolution necessitated modifications to the algorithm to avoid occasional classifications of the entire stratosphere as high-PV surface-connected (therefore tropospheric) air (see details in Supplementary Information). Comparing folding identification with versus without our modifications shows them to be generally conservative, reducing folding frequency (Figure S1).

Analysis year 2012 was chosen in order to minimize discontinuities in assimilated ozone data and provide the most recent data free of known instrumentation biases (affecting CAMSRA ozone from 2013 onwards; Inness et al., 2019; Wagner et al., 2021). Folding frequencies in 2012 are roughly consistent with the 1979–2014 average (from ERA-Interim; Figure S1). Because a single year was used, ozone and folding fields were deseasonalized by removing smoothed local monthly averages before correlation analysis.

3 Results

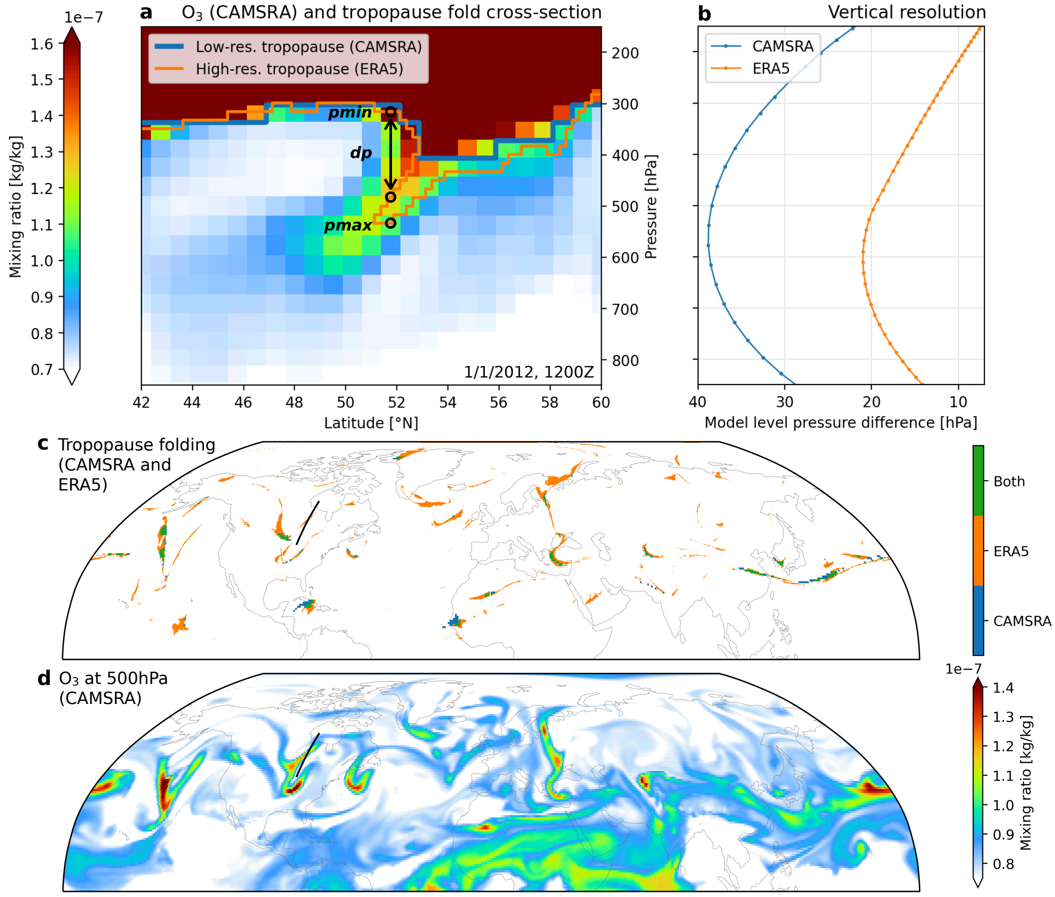

Figure 1. Comparison of a tropopause fold cross-section, vertical resolution, and snapshot folding and mid-tropospheric ozone in CAMSRA and ERA5. ***a)***: Dynamical tropopauses in CAMSRA and ERA5, and ozone from CAMSRA, along a latitudinal cross-section (line in ***c*–*d)***) on 1/1/2012 (1200Z). The ERA5 tropopause is folded throughout a range of columns ($\sim 51°$–$53°$N); pressure parameters *pmin*, *dp*, and *pmax* produced by the folding identification algorithm (see Data and Methods) are illustrated for one column. ***b)***: CAMSRA and ERA5 vertical resolution; dots indicate model levels. ***c*–*d)***: All columns with folding identified in CAMSRA, ERA5, or both (***c)***), and 500 hPa ozone (***d)***), during the example timestep.

We first show an example of tropopause folding captured only at higher resolution: a latitudinal cross-section displays a fold in the ERA5 tropopause that CAMSRA's tropopause is too coarse to resolve (Figure 1a). Meanwhile, in this fold's vicinity, ozone (in CAMSRA) intrudes from the stratosphere into the troposphere—hence, while the intrusion itself is resolved by CAMSRA, its relationship to folding is only captured by a higher-resolution tropopause. More broadly, during the example timestep, folding is much more widespread in ERA5, and reveals stronger correspondence with mid-tropospheric ozone, overlapping with many filamentary ozone structures that CAMSRA folding does not (Figure 1c–d). This improved correspondence generally persists across the 250, 500, and 850 hPa levels for both total (O_3) and stratosphere-sourced (O_3S) ozone, although the general folding–ozone relationship weakens in the tropics and at 850 hPa (Figure S2). This cross-section suggests an important role for vertical resolution—accordingly, ERA5's is at least roughly double CAMSRA's throughout the troposphere (Figure 1b)—while a geographic perspective also emphasizes horizontal resolution (Figure 1c–d). Overall, it appears common that ozone intrusions are only revealed to be associated with folding when the tropopause is seen at high-enough resolution. In such cases, the transport itself occurs at scales larger than the ERA5-identified folding—CAMSRA ozone is advected by resolved winds—entering the troposphere despite an unfolded (coarsely-resolved) tropopause. (Meanwhile, it is possible that alternative tropopause definitions may identify folding in better alignment with transport at lower resolution, especially if based on tracers, but this is beyond our scope).

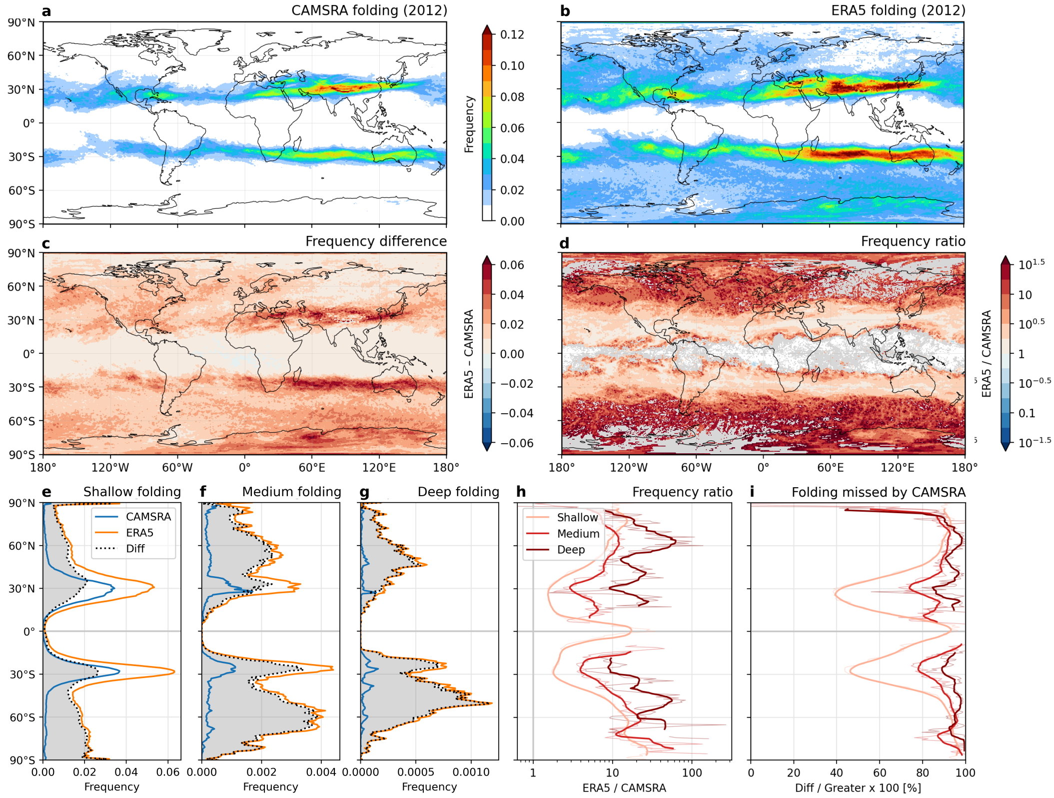

Figure 2. One-year tropopause folding frequencies in CAMSRA and ERA5. ***a–b)***: Folding frequency throughout 2012, in fractional units (0.1 = 36.5 days per year). ***c–d)***: Frequency difference (ERA5 – CAMSRA) and ratio (ERA5 / CAMSRA). ***e–g)***: Zonal-mean frequency of Shallow, Medium, and Deep folding (note x-axis scales). ***h–i)***: Zonal-mean frequency ratio and percentage of folding missed by the lower-frequency dataset (i.e., the frequency difference in ***c)*** as a percentage of the greater of the two at each grid cell) separated by depth range, with running 10° means.

Expanding our analysis to one year, we find that folding frequency increases nearly everywhere from CAMSRA to ERA5 (Figure 2a–c). Vertical resolution likely plays an important role: folds are more often below model-level resolution in CAMSRA than ERA5, with ERA5 folds largely occurring at resolved scales (Figure S3). Their frequency difference (Figure 2c) resembles the underlying distributions (largest along the subtropical jets [STJs], especially over the South Indian Ocean, Middle East, and North Africa), most closely mirroring ERA5's. However, relative frequency differences (Figure 2d) reveal where CAMSRA particularly under-represents folding, highlighting areas with generally rarer folding. Over much of the extratropics, folding increases >10-fold between datasets; many areas with zero CAMSRA folding approach 2% in ERA5. Additionally, while absolute frequency increases are largest for shallower folds (due to their greater prevalence), relative increases are strongest for deeper folds (Figure 2e–i). Furthermore, zonal-mean distributions of Medium and Deep folding in CAMSRA fail to capture to first order their prominent midlatitude peaks evident in ERA5. Zonal-mean frequency ratio (Figure 2h) and percentage of ERA5 folding missed by CAMSRA (Figure 2i) confirm that deeper folding is more likely to be uncaptured at low resolution. Specifically, while around half of ERA5 folding is missed by CAMSRA at its dominant latitudes (rising to >90% in the extratropics and overall nearly 90% on average), nearly 100% of Deep folding is missed almost everywhere (Figure 2i, S4).

The finding that lower resolution disproportionately misses deeper folding likely reflects that as intrusions extend deeper into the troposphere they tend to become more filamentary, hence more difficult to resolve vertically. Accordingly, the distribution of average folding depth (Figure S5) very strongly predicts that of frequency ratio (Figure 2d). Such an underestimation of specifically deeper intrusions into the troposphere may be consequential towards capturing folding's relationship with tropospheric ozone: therefore, we next investigate the influence of folding resolution on temporal correlations between folding activity and ozone STT.

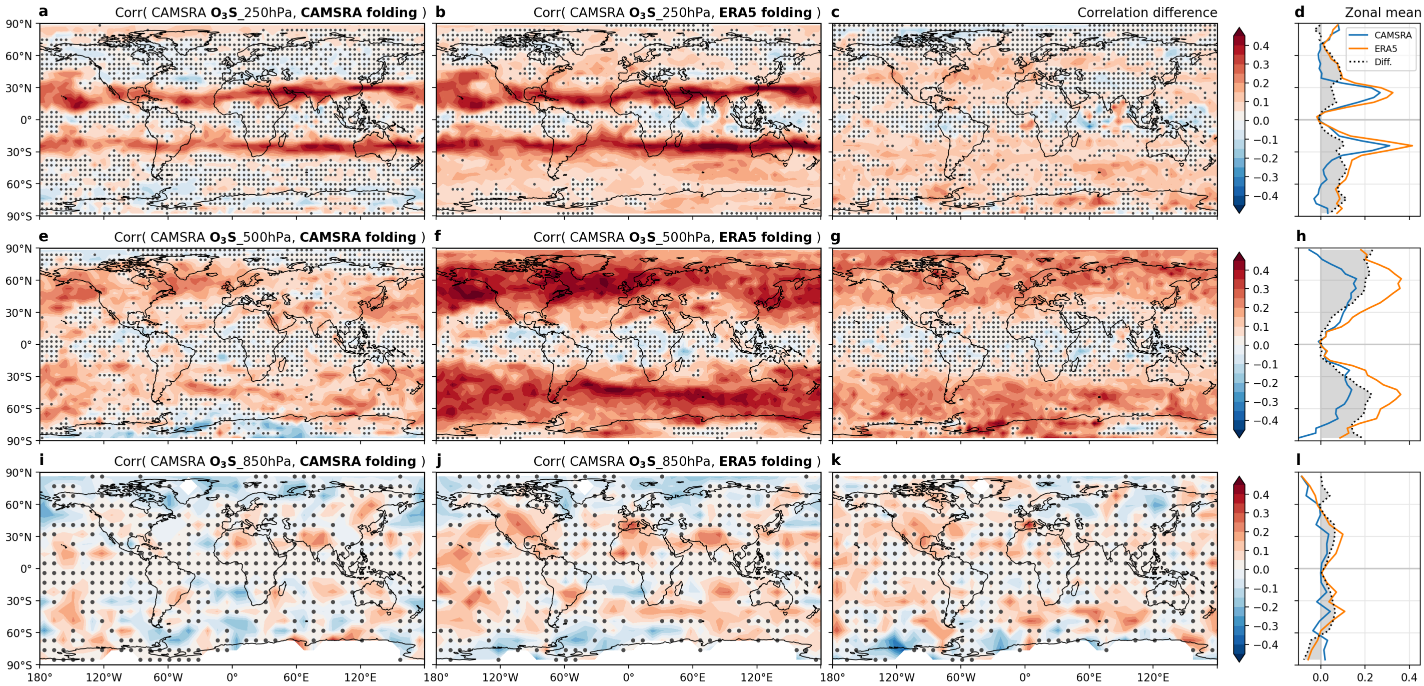

Figure 3. Correlations between tropopause folding and CAMSRA ozone at three pressure levels. ***a)***: Spearman's rank correlation between folding occurrence in CAMSRA and stratospheric ozone tracer (O_3S, from CAMSRA) at 250 hPa, throughout 2012, dotted where insignificant ($\alpha = 0.05$). ***b)***: As in ***a)*** but for ERA5 folding. In other words, between **a)** and **b)** the same O_3S field is correlated against two different folding fields. ***c)***: Difference in correlation coefficients, dotted where insignificant. ***d)***: Zonal means of ***a–c)***. ***e–l)***: As in ***a–d)*** but for O_3S at 500 and 850 hPa. Fields are coarsened to $4.5° \times 4.5°$ (250, 500 hPa) or $9° \times 9°$ (850 hPa), and smoothed by one-day (500 hPa) or three-day (850 hPa) running means, to better capture non-local ozone impacts of folding; only Medium and Deep folding is considered at 850 hPa.

Accompanying increased fold frequency with increased resolution, the correlation between folding and tropospheric O_3S (to most directly reflect STT) significantly strengthens, outside the tropics (Figure 3). The relationship between folding and 250 hPa O_3S closely follows underlying fold frequency distributions (Figure 2a–b, e): correlation maximizes along STJs, reaching 0.40 for CAMSRA and 0.45 for ERA5, and generally strengthens with higher folding frequency (Figure 3a–d). However, correlations strengthen most where relative (Figure 2d) rather than absolute (Figure 2c) frequency differences are highest, increasing by $\sim$0.2 from near-zero in CAMSRA throughout much of the extratropics (where 250 hPa most represents the upper troposphere / lower stratosphere region).

At 500 hPa, O_3S is most correlated to folding in the extratropics, emphasizing storm tracks rather than STJs (Figure 3e–f, h). Correlations strongly mirror folding depth (Figure S5), implying that deeper midlatitude folds, though rarer than STJ-related folds, are more powerfully associated with mid-tropospheric ozone. O_3S at 500 hPa is roughly twice as correlated to ERA5 folding as to CAMSRA folding, reaching $\sim$0.4 over widespread regions, and correlation improvements again reflect relative frequency increases, as well as Medium and Deep folding differences (Figure S6). At 850 hPa, O_3S is much less correlated with folding overall (Figure 3i–j, l), perhaps partially reflecting that folding-related ozone impacts may be spatially offset from folding itself after transport into the lower troposphere. However, O_3S correlation with ERA5 folding reveals maxima in known hotspots of strong stratospheric and folding influence on near-surface ozone (not well captured by CAMSRA folding), including western North America, the Tibetan Plateau, the Mediterranean, and storm track regions (Skerlak et al., 2014). Increases in correlation generally follow Medium and Deep fold frequency increases—strongest over North America and the eastern Pacific and Southern Ocean storm tracks (Figure 3k).

Since O_3S's stronger relation to ERA5 than CAMSRA folding occurs alongside *more frequent* folding, we argue that ozone STT may be more attributable to folding than low-resolution folding implies. In other words, ozone STT occurring without folding in CAMSRA is revealed to occur in the vicinity of folding at smaller scales, as suggested by Figure 1. Altogether, correlations strengthen most at the approximate latitudes of maximum ozone STT—in midlatitudes, poleward of STJs (Hsu & Prather, 2009; Skerlak et al., 2014)—implying the relevance of these changes for overall STT. Furthermore, Figure 3's correlation results are generally consistent when substituting total ozone for O_3S, (Figure S7)—except at 850 hPa, where its drivers are very diverse—suggesting that folding-related O_3S is important to total (free-tropospheric) ozone.

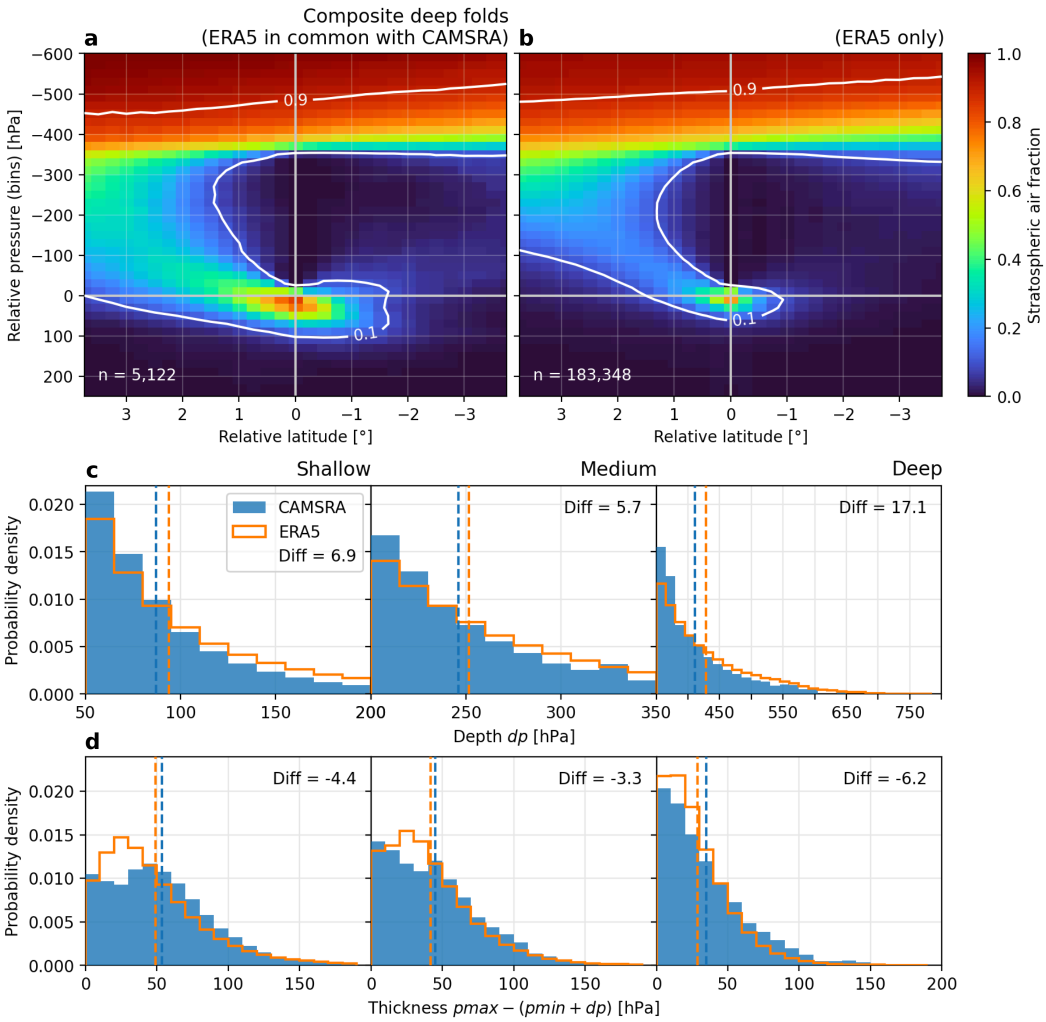

Figure 4. **Tropopause folding morphology in CAMSRA and ERA5.** ***a–b)***: Composited latitudinal cross-sections of Deep folds in ERA5 (i.e., throughout ranges of columns where folding depth dp exceeds 350 hPa, centered horizontally on the column of smallest dp and vertically on that column's middle tropopause crossing), for folding identified in both ERA5 and CAMSRA simultaneously (***a)***) versus only in ERA5 (***b)***). The composited field is a binary label delineating troposphere (0) versus stratosphere (1), producing an average fold morphology; 0.1 and 0.9 contours are indicated. ***c)***: Histograms of dp for folding in CAMSRA and ERA5 in each depth category, with means compared. ***d)***: As in ***c)*** but for folding thickness (the pressure difference between the lowest and middle tropopause crossings, $pmax - (pmin + dp)$).

Following Figure 3's suggestion of deeper folding's role in strengthening ozone correlations, we directly investigate fold morphology, confirming that higher-resolution folding is both deeper and thinner, especially for Deep folding (Figure 4). Composites of ∼190,000

Deep fold cross-sections in ERA5 compare folding captured by both CAMSRA and ERA5 with that only captured by ERA5 (Figure 4a–b). To compare fold morphology, we composite a binary label field that geometrically delineates the stratosphere and troposphere. Cross-sections are fixed around folds' column of minimum depth (exceeding 350 hPa) and their middle tropopause crossing in that column (see Figure 4 caption), so that fold depth (negative pressures) and thickness (positive pressures) can both be compared across cross-sections. These cross-sections capture only folds' latitudinal component; however, we note that even primarily-longitudinal folds likely still express in latitude (e.g., Figure 1's example). From CAMSRA to ERA5, the 0.1 (90% stratospheric) contour thins everywhere along the composite fold, indicating decreased thickness—meanwhile, the 0.9 contour rises further above the fold, indicating increased depth (Figure 4a). Moreover, depth and thickness histograms (Figure 4c–d) quantitatively confirm that with increasing resolution, folding becomes deeper but thinner, consistently across folding depth categories (geospatially resolved in Figure S8). Deep folding is most affected, becoming on average 17 hPa deeper and 6 hPa thinner. Furthermore, in columns where ERA5 identifies Deep folding but CAMSRA fails, CAMSRA almost exclusively identifies no folding rather than simulating Medium or Shallow folding (Figure S9), confirming that CAMSRA specifically underresolves the tips of intrusions.

Figure 4 therefore provides evidence that resolving deeper, thinner folding is particularly responsible for uncovering stronger relationships between folding and tropospheric ozone. Specifically, with higher-resolution folding, ozone anomalies at greater distance from the tropopause may remain attributable to folding activity, as epitomized by Figure 1a's cross-section: the fold tip in ERA5 extends deeper than in CAMSRA (which finds no fold), overlapping with more of the underlying ozone intrusion and thereby revealing that deeper parts of it are attributable to folding.

4 Conclusions and Discussion

In this study, we identified tropopause folding in two reanalyses—high-resolution ERA5 and lower-resolution chemical reanalysis CAMSRA (providing nearly identical meteorology but at the resolution of ERA-Interim). We compared the distribution and characteristics of folding in ERA5 (the highest-resolution such analysis to date) to those in CAMSRA, and assessed the relationships of folding at both resolutions with tropospheric ozone (from CAMSRA), to examine folding's role in the behavior of tropospheric ozone and its transport from the stratosphere. Our conclusions and their implications are as follows:

1. Higher-resolution folding is markedly more frequent. Between datasets, frequency increases most along the subtropical jets and for shallower folds, but increases *relatively* most in the extratropics and for deeper folds (∼10–100-fold). Deep folding is nearly 100% unrepresented at lower resolution, as is ∼90% of all folding.
2. Higher-resolution folding reveals significantly stronger correlations between folding and upper- and mid-tropospheric O_3S (stratospheric ozone tracer), especially where relative fold frequency increases are greatest and folds are deeper.
3. Higher-resolution folding's correlation with near-surface O_3S highlights known hotspots of stratospheric ozone influence uncaptured by low-resolution folding.
4. Correlations of folding with O_3S and with total ozone are largely consistent with each other (above 850 hPa).
5. Increased resolution reveals folding to be deeper and thinner, suggesting that such folding may contribute significantly to folding–ozone correlations.

Together, our results suggest that ozone STT and tropospheric ozone are more systematically associated with tropopause folding than implied based on low-resolution folding. Specifically, of the ozone STT commonly occurring despite an unfolded (coarsely-resolved) tropopause in CAMSRA, much is revealed to be occurring in the vicinity of smaller-scale folding that is only visible at higher resolution. While this work compares one (low-resolution) ozone dataset against two different folding datasets, future work will also assess ozone at high resolution to understand folding-associated STT in greater detail.

While no studies have as comprehensively addressed both folding and its relationship to ozone transport, several have indicated the significance of folding in such processes: localized observational and process-based studies have demonstrated strong ozone STT within intrusions, extending deep into the troposphere, and broader-scale studies have noted the important influence of stratospheric ozone on tropospheric ozone (Langford et al., 1996; Langford & Reid, 1998; Langford et al., 2009; Lefohn et al., 2012; Hess et al., 2015; Neu et al., 2014; Skerlak et al., 2019; Williams et al., 2019; Wang et al., 2020). While folding's importance to STT of air is well established (Stohl et al., 2003), such a systematic linkage to specifically ozone STT is lacking. Here, we provide systematic evidence that higher-resolution folding accounts for a larger proportion of ozone STT than lower-resolution folding. Our findings are specifically consistent with midlatitude-cyclone-associated folding representing a primary STT mechanism (with cyclone dry intrusions previously found to contribute 42% of NH ozone STT; Jaeglé et al., 2017). We show that, although ozone STT is known to be strongest along storm tracks (Skerlak et al., 2014; Hsu & Prather, 2009), its linkage with folding in these areas has remained uncaptured by low-resolution folding climatologies, which underrepresent midlatitude folding due to its smaller scales.

Furthermore, the particular importance of thinner and deeper folding to tropospheric ozone underscores atmospheric transport's filamentary nature. Transport in the stable, highly-sheared free troposphere dominantly occurs in thin layers and plumes that filament, resisting diffusion (Newell et al., 1999; Stoller et al., 1999; Thouret et al., 2000; Heald et al., 2003). Consequently, high-concentration layers are known to enable strong localized stratospheric influence on near-surface (Trickl et al., 2010, 2020) and mid-tropospheric (Trickl et al., 2011) ozone. However, current global models fail to represent transport plumes' observed persistence due to resolution-related over-diffusion (Eastham & Jacob, 2017; Zhuang et al., 2018). Our results imply that such small-scale structures are systematically representative of tropospheric ozone and STT, so that representing such filamentary processes in reanalysis and model simulations is crucial to accurately simulating tropospheric ozone and its transport.

Acknowledgments

This work was supported by NSF Award AGS-1802248 (S. B. and Y. W.) and NSF OPP-1825858 (M. T., Y. W. and C. Z.).

Open Research

Data Availability Statement

All reanalysis data is publicly available from the ECMWF at `https://cds.climate.copernicus.eu/cdsapp#!/dataset/reanalysis-era5-pressure-levels?tab=overview` (ERA5) and `https://ads.atmosphere.copernicus.eu/cdsapp#!/dataset/cams-global-reanalysis-eac4?tab=overview` (CAMSRA). Tropopause folding identification algorithm is available at [insert Zenodo DOI when uploaded]. Code to reproduce the figures and other results is available at [insert Zenodo DOI when uploaded].

References

Akritidis, D., Pozzer, A., Flemming, J., Inness, A., Nédélec, P., & Zanis, P. (2022). A process-oriented evaluation of cams reanalysis ozone during tropopause folds over europe for the period 2003–2018. *Atmospheric Chemistry and Physics Discussions*, 1–23.

Akritidis, D., Pozzer, A., Flemming, J., Inness, A., & Zanis, P. (2021). A global climatology of tropopause folds in cams and merra-2 reanalyses. *Journal of Geophysical Research: Atmospheres*, *126*(8), e2020JD034115. doi: 10.1029/2020JD034115

Akritidis, D., Pozzer, A., & Zanis, P. (2019, Nov). On the impact of future climate change on tropopause folds and tropospheric ozone. *Atmospheric Chemistry and Physics*, *19*(22), 14387–14401. doi: https://doi.org/10.5194/acp-19-14387-2019

Akritidis, D., Pozzer, A., Zanis, P., Tyrlis, E., Škerlak, B., Sprenger, M., & Lelieveld, J. (2016, Nov). On the role of tropopause folds in summertime tropospheric ozone over the eastern mediterranean and the middle east. *Atmospheric Chemistry and Physics*, *16*(21), 14025–14039. doi: 10.5194/acp-16-14025-2016

Appenzeller, C., & Davies, H. C. (1992, Aug). Structure of stratospheric intrusions into the troposphere. *Nature*, *358*(63876387), 570–572. doi: 10.1038/358570a0

Appenzeller, C., Davies, H. C., & Norton, W. A. (1996). Fragmentation of stratospheric intrusions. *Journal of Geophysical Research: Atmospheres*, *101*(D1), 1435–1456. doi: 10.1029/95JD02674

Banerjee, A., Maycock, A. C., Archibald, A. T., Abraham, N. L., Telford, P., Braesicke, P., & Pyle, J. A. (2016, Mar). Drivers of changes in stratospheric and tropospheric ozone between year 2000 and 2100. *Atmospheric Chemistry and Physics*, *16*(5), 2727–2746. doi: 10.5194/acp-16-2727-2016

Beekmann, M., Ancellet, G., Blonsky, S., De Muer, D., Ebel, A., Elbern, H., ... Van Haver, P. (1997, Nov). Regional and global tropopause fold occurrence and related ozone flux across the tropopause. *Journal of Atmospheric Chemistry*, *28*(1), 29–44. doi: 10.1023/A:1005897314623

Buker, M. L., Hitchman, M. H., Tripoli, G. J., Pierce, R. B., Browell, E. V., & Avery, M. A. (2005). Resolution dependence of cross-tropopause ozone transport over east asia. *Journal of Geophysical Research: Atmospheres*, *110*(D3). Retrieved from `https://agupubs.onlinelibrary.wiley.com/doi/abs/10.1029/2004JD004739` doi: https://doi.org/10.1029/2004JD004739

Cariolle, D., & Déqué, M. (1986). Southern hemisphere medium-scale waves and total ozone disturbances in a spectral general circulation model. *Journal of Geophysical Research: Atmospheres*, *91*(D10), 10825–10846. doi: 10.1029/JD091iD10p10825

Cariolle, D., & Teyssèdre, H. (2007, May). A revised linear ozone photochemistry parameterization for use in transport and general circulation models: multi-annual simulations. *Atmospheric Chemistry and Physics*, *7*(9), 2183–2196. doi: 10.5194/acp-7-2183-2007

Chen, X., Añel, J. A., Su, Z., Torre, L. d. l., Kelder, H., Peet, J. v., & Ma, Y. (2013, Feb). The deep atmospheric boundary layer and its significance to the stratosphere and troposphere exchange over the tibetan plateau. *PLOS ONE*, *8*(2), e56909. doi: 10.1371/journal.pone.0056909

Chen, X. L., Ma, Y. M., Kelder, H., Su, Z., & Yang, K. (2011, May). On the behaviour of the tropopause folding events over the tibetan plateau. *Atmospheric Chemistry and Physics*, *11*(10), 5113–5122. doi: 10.5194/acp-11-5113-2011

Danielsen, E. F. (1959, Jun). The laminar structure of the atmosphere and its relation to the concept of a tropopause. *Archiv für Meteorologie, Geophysik und Bioklimatologie, Serie A*, *11*(3), 293–332. doi: 10.1007/BF02247210

Danielsen, E. F. (1968, May). Stratospheric-tropospheric exchange based on radioactivity, ozone and potential vorticity. *Journal of Atmospheric Sciences*, *25*(3), 502–518. doi: 10.1175/1520-0469(1968)025⟨0502:STEBOR⟩2.0.CO;2

Dee, D. P., Uppala, S. M., Simmons, A. J., Berrisford, P., Poli, P., Kobayashi, S., ... others (2011). The ERA-Interim reanalysis: Configuration and performance of the data assimilation system. *Quarterly Journal of the royal meteorological society*, *137*(656), 553–597.

Dragani, R. (2010). *On the quality of the era-interim ozone reanalyses. part ii comparisons with satellite data.* ECMWF.

Eastham, S. D., & Jacob, D. J. (2017, Feb). Limits on the ability of global eulerian models to resolve intercontinental transport of chemical plumes. *Atmospheric Chemistry and Physics*, *17*(4), 2543–2553. doi: 10.5194/acp-17-2543-2017

Flemming, J., Huijnen, V., Arteta, J., Bechtold, P., Beljaars, A., Blechschmidt, A.-M., ... Tsikerdekis, A. (2015, Apr). Tropospheric chemistry in the integrated forecasting system of ecmwf. *Geoscientific Model Development*, *8*(4), 975–1003. doi: 10.5194/gmd-8-975-2015

Fu, T.-M., & Tian, H. (2019, Sep). Climate change penalty to ozone air quality: Review of current understandings and knowledge gaps. *Current Pollution Reports*, *5*(3), 159–171. doi: 10.1007/s40726-019-00115-6

Heald, C. L., Jacob, D. J., Fiore, A. M., Emmons, L. K., Gille, J. C., Deeter, M. N., ... Fuelberg, H. E. (2003). Asian outflow and trans-pacific transport of carbon monoxide and ozone pollution: An integrated satellite, aircraft, and model perspective. *Journal of Geophysical Research: Atmospheres*, *108*(D24). Retrieved from `https://onlinelibrary.wiley.com/doi/abs/10.1029/2003JD003507` doi: 10.1029/2003JD003507

Hegglin, M. I., & Shepherd, T. G. (2009, Oct). Large climate-induced changes in ultraviolet index and stratosphere-to-troposphere ozone flux. *Nature Geoscience*, *2*(10), 687–691. doi: 10.1038/ngeo604

Hersbach, H., Bell, B., Berrisford, P., Hirahara, S., Horányi, A., Muñoz-Sabater, J., ... Thépaut, J.-N. (2020). The era5 global reanalysis. *Quarterly Journal of the Royal Meteorological Society*, *146*(730), 1999–2049. doi: https://doi.org/10.1002/qj.3803

Hess, P., Kinnison, D., & Tang, Q. (2015, Mar). Ensemble simulations of the role of the stratosphere in the attribution of northern extratropical tropospheric ozone variability. *Atmospheric Chemistry and Physics*, *15*(5), 2341–2365. doi:

10.5194/acp-15-2341-2015

Hoffmann, L., & Spang, R. (2022). An assessment of tropopause characteristics of the ERA5 and ERA-Interim meteorological reanalyses. *Atmospheric Chemistry and Physics*, *22*(6), 4019–4046.

Hsu, J., & Prather, M. J. (2009). Stratospheric variability and tropospheric ozone. *Journal of Geophysical Research: Atmospheres*, *114*(D6). Retrieved from `https://onlinelibrary.wiley.com/doi/abs/10.1029/2008JD010942` doi: 10.1029/2008JD010942

Huijnen, V., Williams, J., van Weele, M., van Noije, T., Krol, M., Dentener, F., ... Pätz, H.-W. (2010, Oct). The global chemistry transport model tm5: description and evaluation of the tropospheric chemistry version 3.0. *Geoscientific Model Development*, *3*(2), 445–473. doi: 10.5194/gmd-3-445-2010

Inness, A., Ades, M., Agustí-Panareda, A., Barré, J., Benedictow, A., Blechschmidt, A.-M., ... Suttie, M. (2019, Mar). The cams reanalysis of atmospheric composition. *Atmospheric Chemistry and Physics*, *19*(6), 3515–3556. doi: 10.5194/acp-19-3515-2019

Jaeglé, L., Wood, R., & Wargan, K. (2017). Multiyear composite view of ozone enhancements and stratosphere-to-troposphere transport in dry intrusions of northern hemisphere extratropical cyclones. *Journal of Geophysical Research: Atmospheres*, *122*(24), 13,436-13,457. doi: 10.1002/2017JD027656

Knowland, K. E., Ott, L. E., Duncan, B. N., & Wargan, K. (2017). Stratospheric intrusion-influenced ozone air quality exceedances investigated in the nasa merra-2 reanalysis. *Geophysical Research Letters*, *44*(20), 10,691-10,701. doi: https://doi.org/10.1002/2017GL074532

Krzyzanowski, M., & Cohen, A. (2008, Jun). Update of who air quality guidelines. *Air Quality, Atmosphere & Health*, *1*(1), 7–13. doi: 10.1007/s11869-008-0008-9

Langford, A., Aikin, K., Eubank, C., & Williams, E. (2009). Stratospheric contribution to high surface ozone in Colorado during springtime. *Geophysical Research Letters*, *36*(12).

Langford, A., Masters, C., Proffitt, M., Hsie, E.-Y., & Tuck, A. (1996). Ozone measurements in a tropopause fold associated with a cut-off low system. *Geophysical research letters*, *23*(18), 2501–2504.

Langford, A., & Reid, S. (1998). Dissipation and mixing of a small-scale stratospheric intrusion in the upper troposphere. *Journal of Geophysical Research: Atmospheres*, *103*(D23), 31265–31276.

Lefohn, A. S., Wernli, H., Shadwick, D., Oltmans, S. J., & Shapiro, M. (2012, Dec). Quantifying the importance of stratospheric-tropospheric transport on surface ozone concentrations at high- and low-elevation monitoring sites in the united states. *Atmospheric Environment*, *62*, 646–656. doi: 10.1016/j.atmosenv.2012.09.004

Lin, M., Fiore, A. M., Cooper, O. R., Horowitz, L. W., Langford, A. O., Levy, H., ... Senff, C. J. (2012). Springtime high surface ozone events over the western united states: Quantifying the role of stratospheric intrusions. *Journal of Geophysical Research: Atmospheres*, *117*(D21). Retrieved from `https://agupubs.onlinelibrary.wiley.com/doi/abs/10.1029/2012JD018151` doi: https://doi.org/10.1029/2012JD018151

Lin, M., Fiore, A. M., Horowitz, L. W., Langford, A. O., Oltmans, S. J., Tarasick, D., & Rieder, H. E. (2015, May). Climate variability modulates western us ozone air quality in spring via deep stratospheric intrusions. *Nature Communications*, *6*(11), 7105. doi: 10.1038/ncomms8105

Meul, S., Langematz, U., Kröger, P., Oberländer-Hayn, S., & Jöckel, P. (2018, Jun). Future changes in the stratosphere-to-troposphere ozone mass flux and the contribution from climate change and ozone recovery. *Atmospheric Chemistry and Physics*, *18*(10), 7721–7738. doi: https://doi.org/10.5194/acp-18-7721-2018

Monks, P. S., Archibald, A. T., Colette, A., Cooper, O., Coyle, M., Derwent, R., ... Williams, M. L. (2015, Aug). Tropospheric ozone and its precursors from the urban to the global scale from air quality to short-lived climate forcer. *Atmospheric Chemistry and Physics*, *15*(15), 8889–8973. doi: 10.5194/acp-15-8889-2015

Myhre, G., Shindell, D., Bréon, F.-M., Collins, W., Fuglestvedt, J., Huang, J., ... Zhang, H. (2013). Anthropogenic and natural radiative forcing. In T. F. Stocker et al. (Eds.), *Climate change 2013: The physical science basis. contribution of working group i to the fifth assessment report of the intergovernmental panel on climate change* (pp. 659–740). Cambridge, UK: Cambridge

University Press. doi: 10.1017/CBO9781107415324.018

Neu, J. L., Flury, T., Manney, G. L., Santee, M. L., Livesey, N. J., & Worden, J. (2014, May). Tropospheric ozone variations governed by changes in stratospheric circulation. *Nature Geoscience*, *7*(5), 340–344. doi: 10.1038/ngeo2138

Newell, R. E., Thouret, V., Cho, J. Y. N., Stoller, P., Marenco, A., & Smit, H. G. (1999, Mar). Ubiquity of quasi-horizontal layers in the troposphere. *Nature*, *398*(67256725), 316–319. doi: 10.1038/18642

Newell, R. E., Wu, Z.-X., Zhu, Y., Hu, W., Browell, E. V., Gregory, G. L., ... Liu, S. C. (1996). Vertical fine-scale atmospheric structure measured from nasa dc-8 during pem-west a. *Journal of Geophysical Research: Atmospheres*, *101*(D1), 1943–1960. doi: 10.1029/95JD02613

Park, S., Son, S.-W., Jung, M.-I., Park, J., & Park, S. S. (2020, Aug). Evaluation of tropospheric ozone reanalyses with independent ozonesonde observations in east asia. *Geoscience Letters*, *7*(1), 12. doi: 10.1186/s40562-020-00161-9

Shapiro, M. A. (1980, May). Turbulent mixing within tropopause folds as a mechanism for the exchange of chemical constituents between the stratosphere and troposphere. *Journal of the Atmospheric Sciences*, *37*(5), 994–1004. doi: 10.1175/1520-0469(1980)037⟨0994:TMWTFA⟩2.0.CO;2

Skerlak, B., Pfahl, S., Sprenger, M., & Wernli, H. (2019, May). A numerical process study on the rapid transport of stratospheric air down to the surface over western north america and the tibetan plateau. *Atmospheric Chemistry and Physics*, *19*(9), 6535–6549. doi: 10.5194/acp-19-6535-2019

Skerlak, B., Sprenger, M., Pfahl, S., Tyrlis, E., & Wernli, H. (2015). Tropopause folds in era-interim: Global climatology and relation to extreme weather events. *Journal of Geophysical Research: Atmospheres*, *120*(10), 4860–4877. doi: https://doi.org/10.1002/2014JD022787

Skerlak, B., Sprenger, M., & Wernli, H. (2014, Jan). A global climatology of stratosphere–troposphere exchange using the era-interim data set from 1979 to 2011. *Atmospheric Chemistry and Physics*, *14*(2), 913–937. doi: https://doi.org/10.5194/acp-14-913-2014

Spreitzer, E., Attinger, R., Boettcher, M., Forbes, R., Wernli, H., & Joos, H. (2019). Modification of potential vorticity near the tropopause by nonconservative processes in the ECMWF model. *Journal of the atmospheric sciences*, *76*(6), 1709–1726.

Sprenger, M., Maspoli, M. C., & Wernli, H. (2003). Tropopause folds and cross-tropopause exchange: A global investigation based upon ecmwf analyses for the time period march 2000 to february 2001. *Journal of Geophysical Research: Atmospheres*, *108*(D12). Retrieved from `https://agupubs.onlinelibrary.wiley.com/doi/abs/10.1029/2002JD002587\%4010.1002/\%28ISSN\%292169-8996.STACCATO1` doi: https://doi.org/10.1029/2002JD002587

Stohl, A., Bonasoni, P., Cristofanelli, P., Collins, W., Feichter, J., Frank, A., ... Zerefos, C. (2003). Stratosphere-troposphere exchange: A review, and what we have learned from staccato. *Journal of Geophysical Research: Atmospheres*, *108*(D12). Retrieved from `https://agupubs.onlinelibrary.wiley.com/doi/abs/10.1029/2002JD002490\%4010.1002/\%28ISSN\%292169-8996.STACCATO1` doi: https://doi.org/10.1029/2002JD002490

Stoller, P., Cho, J. Y. N., Newell, R. E., Thouret, V., Zhu, Y., Carroll, M. A., ... Sandholm, S. (1999). Measurements of atmospheric layers from the nasa dc-8 and p-3b aircraft during pem-tropics a. *Journal of Geophysical Research: Atmospheres*, *104*(D5), 5745–5764. doi: 10.1029/98JD02717

Thouret, V., Cho, J. Y. N., Newell, R. E., Marenco, A., & Smit, H. G. J. (2000). General characteristics of tropospheric trace constituent layers observed in the mozaic program. *Journal of Geophysical Research: Atmospheres*, *105*(D13), 17379–17392. doi: 10.1029/2000JD900238

Trickl, T., Bärtsch-Ritter, N., Eisele, H., Furger, M., Mücke, R., Sprenger, M., & Stohl, A. (2011, Sep). High-ozone layers in the middle and upper troposphere above central europe: potential import from the stratosphere along the subtropical jet stream. *Atmospheric Chemistry and Physics*, *11*(17), 9343–9366. doi: 10.5194/acp-11-9343-2011

Trickl, T., Feldmann, H., Kanter, H.-J., Scheel, H.-E., Sprenger, M., Stohl, A., & Wernli, H. (2010, Jan). Forecasted deep stratospheric intrusions over central europe: case studies and climatologies. *Atmospheric Chemistry and Physics*, *10*(2), 499–524. doi: 10.5194/acp-10-499-2010

Trickl, T., Vogelmann, H., Ries, L., & Sprenger, M. (2020, Jan). Very high stratospheric influence observed in the free troposphere over the northern alps – just a local phenomenon? *Atmospheric Chemistry and Physics*, *20*(1), 243–266.

doi: 10.5194/acp-20-243-2020

Tyrlis, E., Skerlak, B., Sprenger, M., Wernli, H., Zittis, G., & Lelieveld, J. (2014). On the linkage between the asian summer monsoon and tropopause fold activity over the eastern mediterranean and the middle east. *Journal of Geophysical Research: Atmospheres*, *119*(6), 3202–3221. doi: https://doi.org/10.1002/2013JD021113

Wagner, A., Bennouna, Y., Blechschmidt, A.-M., Brasseur, G., Chabrillat, S., Christophe, Y., ... Zerefos, C. (2021, May). Comprehensive evaluation of the copernicus atmosphere monitoring service (cams) reanalysis against independent observations: Reactive gases. *Elementa: Science of the Anthropocene*, *9*(1), 00171. doi: 10.1525/elementa.2020.00171

Wang, X., Wu, Y., Randel, W., & Tilmes, S. (2020, Oct). Stratospheric contribution to the summertime high surface ozone events over the western united states. *Environmental Research Letters*, *15*(10), 1040a6. doi: 10.1088/1748-9326/abba53

Wargan, K., Labow, G., Frith, S., Pawson, S., Livesey, N., & Partyka, G. (2017, Apr). Evaluation of the ozone fields in nasa's merra-2 reanalysis. *Journal of Climate*, *30*(8), 2961–2988. doi: 10.1175/JCLI-D-16-0699.1

Williams, R. S., Hegglin, M. I., Kerridge, B. J., Jöckel, P., Latter, B. G., & Plummer, D. A. (2019, Mar). Characterising the seasonal and geographical variability in tropospheric ozone, stratospheric influence and recent changes. *Atmospheric Chemistry and Physics*, *19*(6), 3589–3620. doi: 10.5194/acp-19-3589-2019

Zanis, P., Hadjinicolaou, P., Pozzer, A., Tyrlis, E., Dafka, S., Mihalopoulos, N., & Lelieveld, J. (2014, Jan). Summertime free-tropospheric ozone pool over the eastern mediterranean/middle east. *Atmospheric Chemistry and Physics*, *14*(1), 115–132. doi: 10.5194/acp-14-115-2014

Zhuang, J., Jacob, D. J., & Eastham, S. D. (2018, May). The importance of vertical resolution in the free troposphere for modeling intercontinental plumes. *Atmospheric Chemistry and Physics*, *18*(8), 6039–6055. doi: 10.5194/acp-18-6039-2018

Supporting Information for "Higher-resolution tropopause folding accounts for more stratospheric ozone intrusions"

Samuel Bartusek[1,2], Yutian Wu[1], Mingfang Ting[1,2], Cheng Zheng[1], Arlene Fiore[3], Michael Sprenger[4], Johannes Flemming[5]

[1]Lamont-Doherty Earth Observatory, Columbia University, Palisades, NY, USA

[2]Department of Earth and Environmental Sciences, Columbia University, New York, NY, USA

[3]Department of Earth, Atmospheric, and Planetary Sciences, Massachusetts Institute of Technology, Cambridge, MA, USA

[4]Institute for Atmosphere and Climate Science, ETH Zürich, Zürich, Switzerland

[5]European Centre for Medium-Range Weather Forecasts (ECMWF), Reading, UK

Contents of this file

1. Text S1
2. Figures S1 to S8

Introduction

This file contains a text section providing details of the modifications we made to the tropopause folding algorithm, and a Supplementary Figures section containing seven figures mentioned in the main article.

Text S1

The folding algorithm we apply to CAMSRA and ERA5 is based on the algorithm originally developed by Sprenger, Maspoli, and Wernli (2003) and further sophisticated by Skerlak, Sprenger, and Wernli (2014) (the labelling portion of the algorithm) and Skerlak, Sprenger, Pfahl, Tyrlis, and Wernli (2015). Its labelling routine produces a label from 1–5 for each grid cell (in 3-D) at each timestep. As alluded to in the main text, these labels geometrically separate grid cells as belonging to either the troposphere or stratosphere, mostly based on their potential vorticity (PV) value but with a few exceptions where PV cannot itself determine which body a certain grid cell belongs to. The labels correspond as follows: 1, troposphere; 2, stratosphere; 3; stratospheric cutoff or diabatically produced PV anomaly; 4, tropospheric cutoff; 5, surface-bound cyclonic PV anomaly. Labels 1, 3, and 5 therefore constitute the troposphere and labels 2 and 4 constitute the stratosphere, where labels 3, 4, and 5 designate the exceptions with PV not indicative of its surrounding body. See Skerlak et al. (2015) for further details.

As mentioned in the main text, it was necessary to make modifications to successfully apply it to ERA5 data. We found that because of ERA5's very high resolution it was susceptible to finding pathways of high-PV air connecting the stratosphere all the way to the surface that are thin enough to be obscured at lower resolution. For such timesteps, the entire stratosphere would constitute a single surface-connected high-PV region, thus receiving label 5 (troposphere), and folding identification would be disallowed anywhere due to filters that help avoid spurious fold identification (see Skerlak et al. (2015) for details of such spurious cases that justify the filters).

The spread of label 5 into the stratosphere was partly attributable to the algorithm's strategy of horizontally propagating labels 5 and 3 into areas of label 2, as long as the area of label 2 is connected to a label 5 grid cell at a higher level. In ERA5 this allowed a single area of label 5 high up in the atmosphere at any location to propagate very extensively horizontally and downward. Our first modification was to deactivate this horizontal propagation behavior, which was introduced for mostly aesthetic reasons in the first place. Specifically, if one compares Figure 1 in Skerlak et al. (2014) against Figure 1 in Skerlak et al. (2015), this behavioral change between the two iterations is responsible for the label 2 "stratospheric funnel" seen in Skerlak et al. (2014) (where label 2 extends through the label 5 blob all the way to the surface) instead being "filled in" with label 5, such that label 5 propagates up to the level of thinnest funnel diameter, as seen in Skerlak et al. (2015).

However, despite this modification, label 5 (or 3) could still sometimes spuriously propagate throughout the stratosphere, invalidating some timesteps. We therefore introduced new conditions to replace appropriate label 5/3 regions that are connected to the stratosphere with label 2, but adopted three conditions to ensure conservativeness.

1. We first impose a condition that such a label 5/3 parcel must be within the upper half of the troposphere (i.e., if a grid cell's pressure distance from the local tropopause is smaller than that from the surface). This condition is very similar to one introduced in Skerlak et al. (2014) wherein label 2 was allowed to propagate horizontally (if contacting label 5) only in the upper half of the troposphere. We lift this lower-troposphere restriction for the approximate Tibetan Plateau region (25°–40°N, 75°–110°E)—its close surface

proximity to the tropopause means that even label 5 regions in the lower troposphere can lead to stratospheric label 5 propagation and missed fold identification (nevertheless, we still find very small to zero frequency differences between CAMSRA and ERA5 in this region (see Figure 2), which by comparisons of cases seems likely to somewhat represent a masking of otherwise increased ERA5 folding frequency, due to persisting spurious label 5 propagation—the frequency differences in this region shown in the main text are therefore likely conservative).

2. Additionally, we only allow relabelling of 5/3 to 2 if the tropopause is greater than 200 hPa from the surface, which for example helps avoid spurious fold identification in winter in Antarctica where very low tropopause heights and high topography with strong surface cooling can create high-PV layers correctly assigned label 5, as discussed in Skerlak et al. (2015).

3. Finally, we modified the algorithm's usage of specific humidity as an indicator of stratospheric air. In the version in Skerlak et al. (2015), as shown in their Figure 4, the threshold $q = 0.1$ g kg^{-1} helps separate low-altitude high-PV airmasses (moist tropospheric air) that merge with a real fold (dry stratospheric air), by determining a level up to which label 5/3 can propagate. Here, we use this threshold in a more restrictive way as a third condition. We disallow any relabelling from 5/3 to 2 for grid cells exceeding it, and we furthermore relabel all cells labelled 2 exceeding it to 5/3—essentially, we use the threshold as a 3-D contour outside of which label 2 is never allowed, as opposed to a vertical level affecting the relabelling of 2 to 5/3, which permitted label 2 to sometimes persist into air moister than the threshold.

As seen in Figure S1 below, our modifications altogether produce a dominantly conservative effect on folding frequencies, for Medium and Deep folding in particular. Our final modified version of the algorithm (specifically, a Fortran code file containing both the 3-D labelling routine and the tropopause fold detection routine based on that label field) is available at [*insert Zenodo link*].

References

Skerlak, B., Sprenger, M., Pfahl, S., Tyrlis, E., & Wernli, H. (2015). Tropopause folds in era-interim: Global climatology and relation to extreme weather events. *Journal of Geophysical Research: Atmospheres*, *120*(10), 4860–4877. doi: https://doi.org/10.1002/2014JD022787

Skerlak, B., Sprenger, M., & Wernli, H. (2014, Jan). A global climatology of stratosphere–troposphere exchange using the era-interim data set from 1979 to 2011. *Atmospheric Chemistry and Physics*, *14*(2), 913–937. doi: https://doi.org/10.5194/acp-14-913-2014

Sprenger, M., Maspoli, M. C., & Wernli, H. (2003). Tropopause folds and cross-tropopause exchange: A global investigation based upon ecmwf analyses for the time period march 2000 to february 2001. *Journal of Geophysical Research: Atmospheres*, *108*(D12). Retrieved from `https://agupubs.onlinelibrary.wiley.com/doi/abs/10.1029/2002JD002587\%4010.1002/\%28ISSN\%292169-8996.STACCATO1` doi: https://doi.org/10.1029/2002JD002587

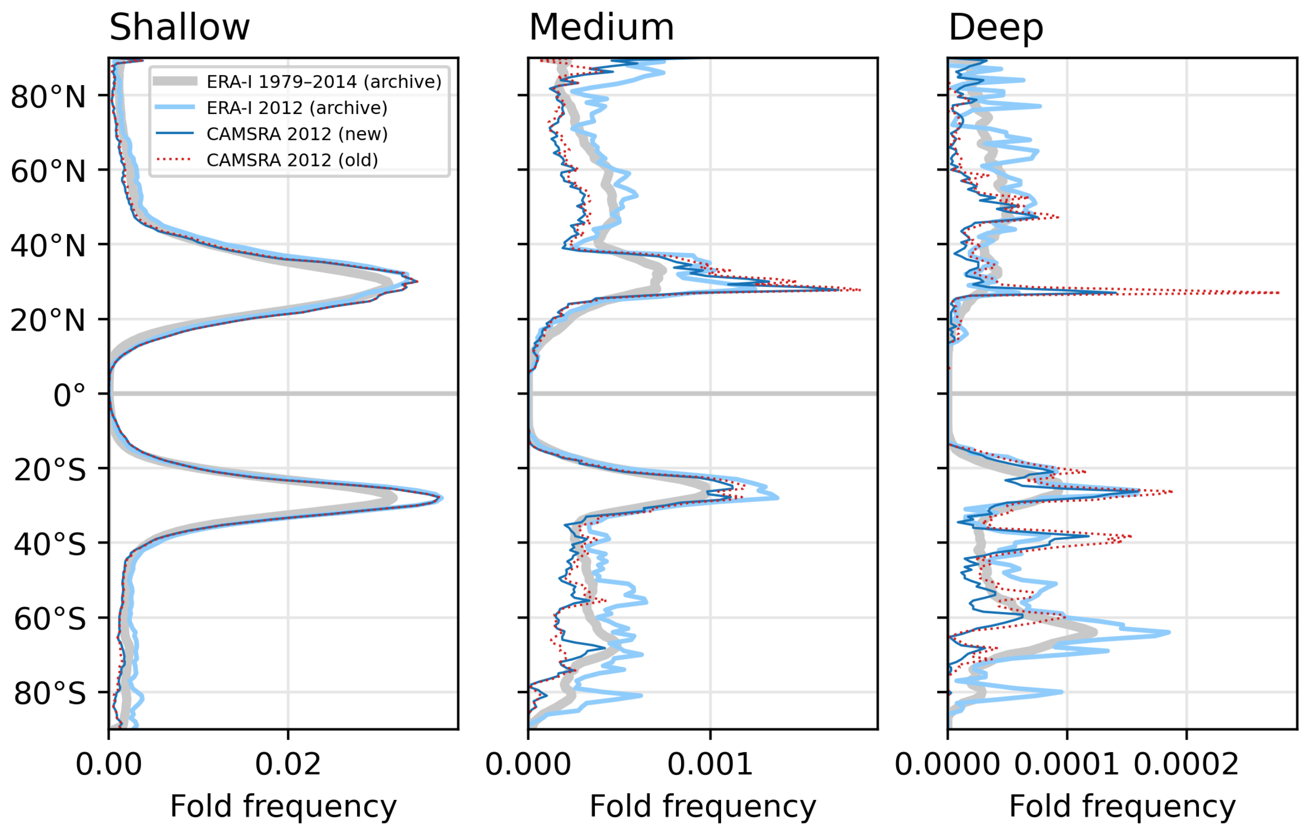

Figure S1. Comparison of 2012 folding to other years, and between folding detection algorithms. ***Left to right***: Zonal-mean fold frequencies are shown for each depth category. The thick light gray line shows the zonal mean tropopause folding frequency over 1979–2014 in ERA-Interim, provided by the ETH Zürich archive (available at http://eraiclim.ethz.ch/). The light blue line isolates the year 2012, showing that 2012 is representative of the underlying average frequency. The dotted red line shows the zonal average frequencies over 2012 in CAMSRA, generated by a newer version of the 3-D labelling algorithm (from Skerlak et al. (2015)). This version introduced more conservativeness in identifying folds than previous versions, likely accounting for most of the difference between it and the ERA-Interim 2012 frequencies (light blue), since the ERA-Interim and CAMSRA meteorologies were produced by the same model (IFS, albeit different model cycles) and at the same resolution. The differences are almost everywhere a reduction in frequency, and are proportionately stronger for Medium and Deep folds. Finally, the dark blue line shows frequencies over 2012 in CAMSRA generated by our modified version of the algorithm, showing that our edits were conservative, reducing frequency nearly everywhere compared with the dotted red line.

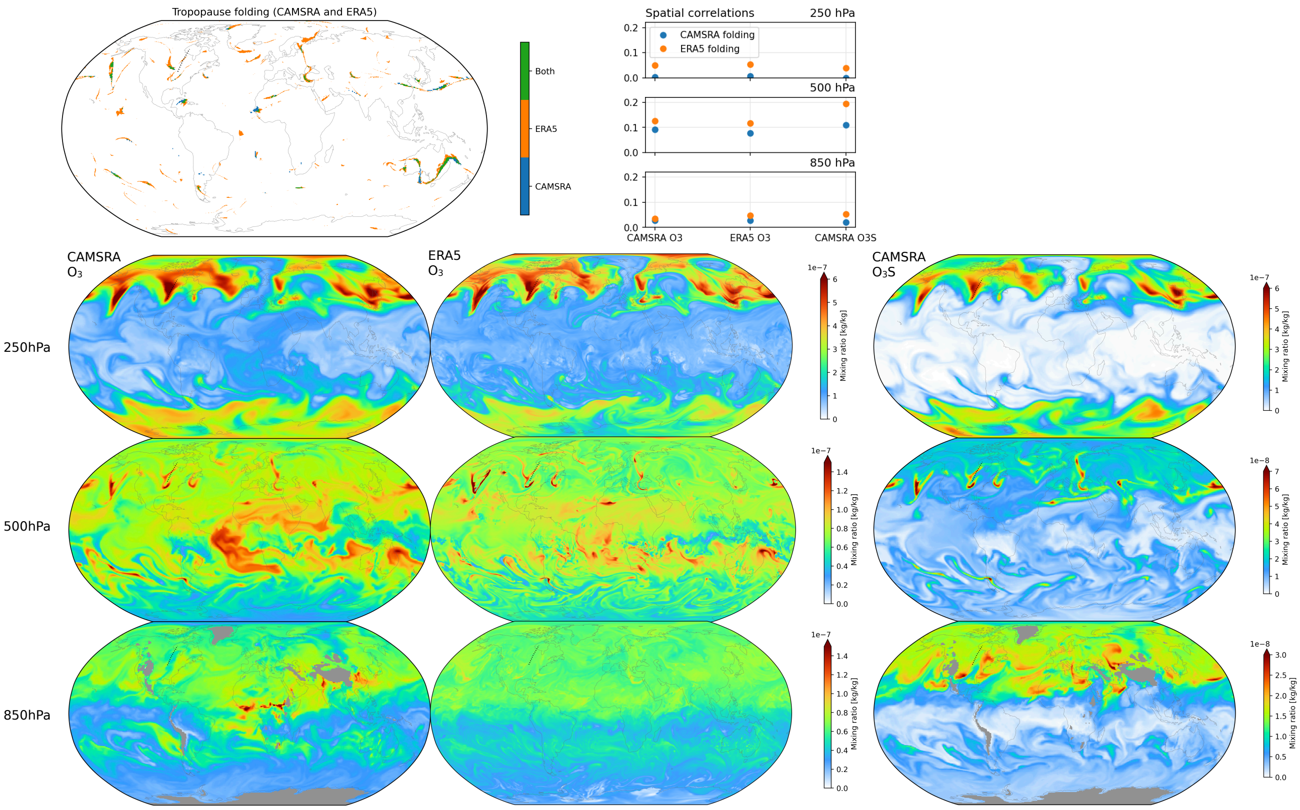

Figure S2. **Folding and ozone snapshots at various levels from CAMSRA and ERA5.** ***Top left:*** Tropopause folding in both CAMSRA and ERA5 on 1/1/2012 at 1200Z (same timestep as Figure 1a,c–d). ***Top right:*** For the same timestep, the spatial correlations between CAMSRA folding and each ozone snapshot shown below (blue markers), versus the same with ERA5 folding (orange markers). ***Second row:*** For the same timestep, CAMSRA ozone, ERA5 ozone, and CAMSRA stratospheric ozone tracer O_3S (left to right) at the 250 hPa level. ***Third and fourth rows:*** As in second row but for the 500 and 850 hPa levels. (Top panel and 500 hPa O_3 are as in Figure 1c and d but over the whole globe.)

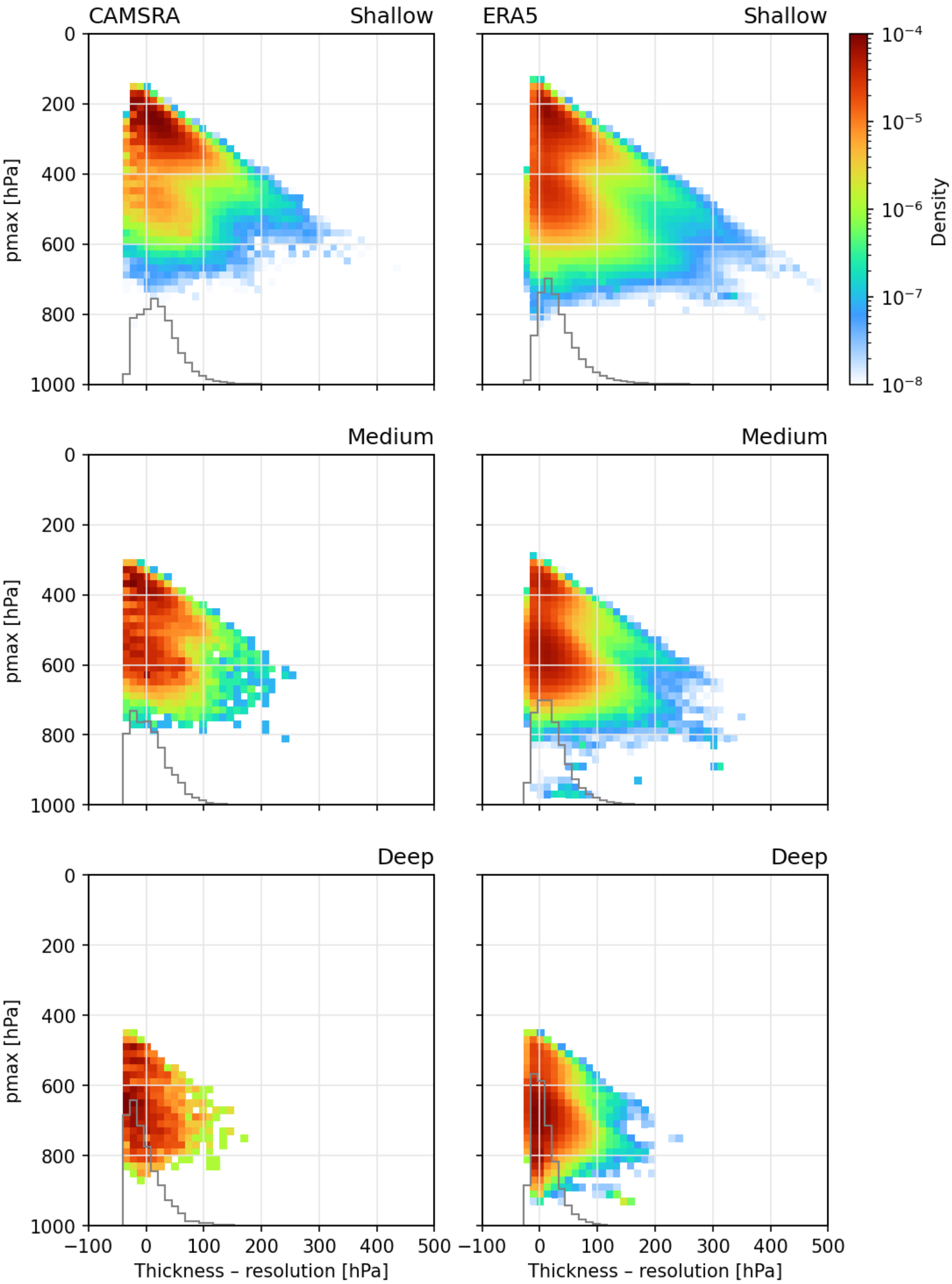

Figure S3. Fold thickness vs. model level resolution. ***Top row:*** For all Shallow folded columns during 2012 in CAMSRA (left) and ERA5 (right), a bivariate density histogram is shown. x-axis: the difference between the fold's vertical thickness ($pmax$–[$pmin$+dp]; see Figure 4) and the model level thickness at the column's lowest tropopause crossing. y-axis: the pressure at the lowest tropopuase crossing ($pmax$). ***Middle and bottom rows:*** Same as top row but for Medium and Deep folding occurrences.

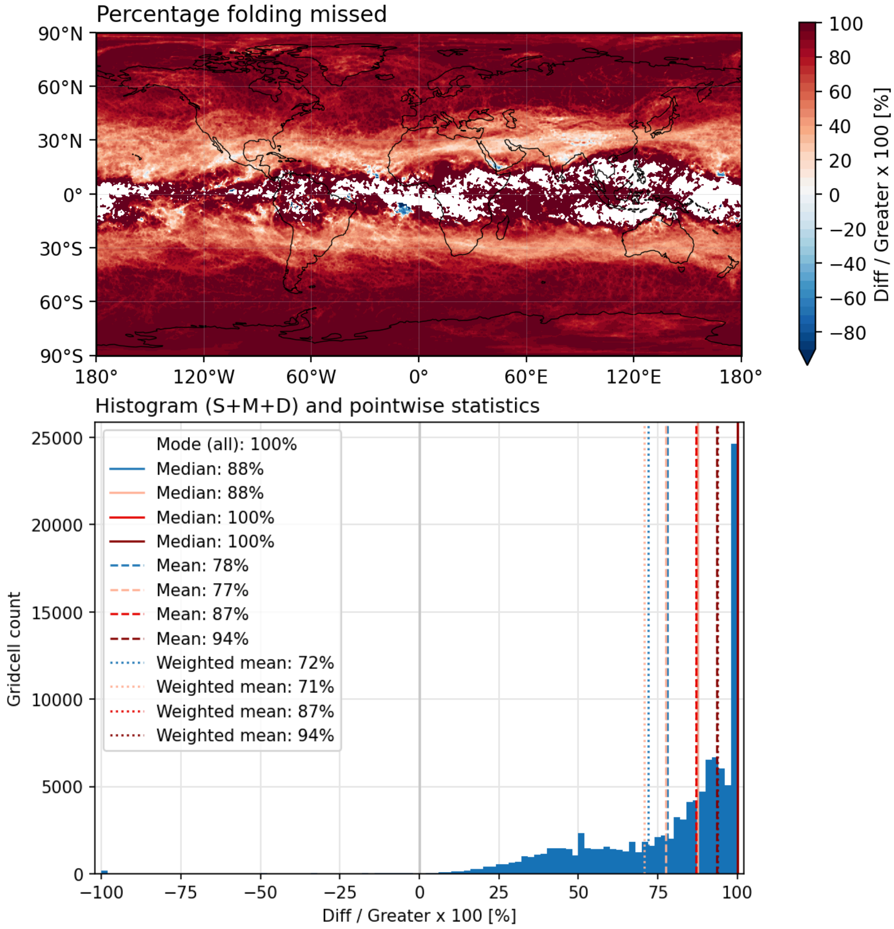

Spatially aggregated statistics

	S+M+D	Shallow	Medium	Deep
(ΣERA5 – ΣCAMSRA) / ΣERA5	68%	66%	85%	93%

Figure S4. Statistics of folding missed by CAMSRA (or ERA5) over 2012. ***Top:*** As in Figure 2i but showing the whole globe instead of a zonal mean. At each gridcell, the percentage of folding in whichever dataset is higher frequency that is missed by whichever dataset is lower frequency (signed positive if ERA5 is higher frequency). In other words, the difference in folding frequency (ERA5 minus CAMSRA), expressed as a percentage of the greater of the two. Areas with no color indicate no folding in either dataset. ***Middle:*** Histogram of all gridcell values in the map above. Statistics are shown in the legend: the modes, medians, means, and area-weighted means for each of the folding depth categories are shown, with accompanying vertical lines (S+M+D, Shallow, Medium, and Deep in blue, pink, red, and dark red). For example, across all gridcells, it is most common for 100% of ERA5 folding at a given location during 2012 to be missed by CAMSRA (i.e., at a given gridcell, CAMSRA folding frequency is zero while ERA5 frequency is non-zero). On average across all locations, nearly 100% of ERA5 Deep folding is missing in CAMSRA (ranging from 94% to 100% by averaging type). ***Bottom:*** Statistics that ignore the location and timing of folding: the total number of CAMSRA folding occurrences over all locations and times in 2012 is compared to that of ERA5, for each depth category. For example, the total number of Deep folded columns is 93% lower in CAMSRA than in ERA5. Note that these sums are taken on the same grid (that of CAMSRA).

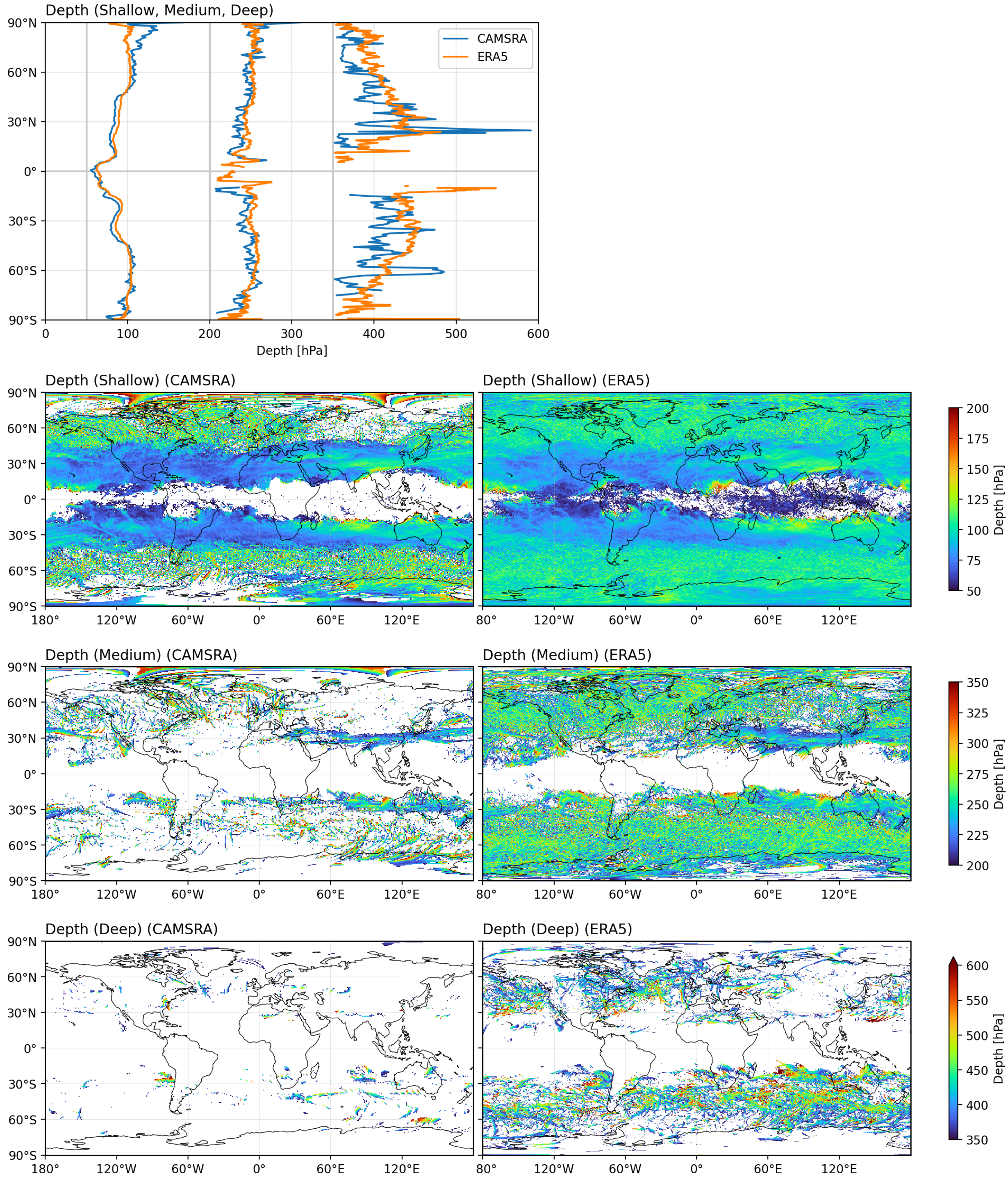

Figure S5. Depth of folding in spatial detail. Depth of folding (dp, see Figure 1a) as in Figure 4c–d's histograms, but shown as zonal means and full maps. ***Top:*** Zonal means of dp in CAMSRA and ERA5 for Shallow, Medium, and Deep folds. x-axis is continuous; gray lines indicate the three depth ranges. ***Second row:*** CAMSRA (left) and ERA5 (right) average folding depths for Shallow folds. White indicates no folding over the whole year. This spatial distribution of depth of Shallow folding tightly mirrors the folding frequency ratio (ERA5/CAMSRA) shown in Figure 1d. ***Third and fourth rows:*** As in second row but for Medium and Deep folding.

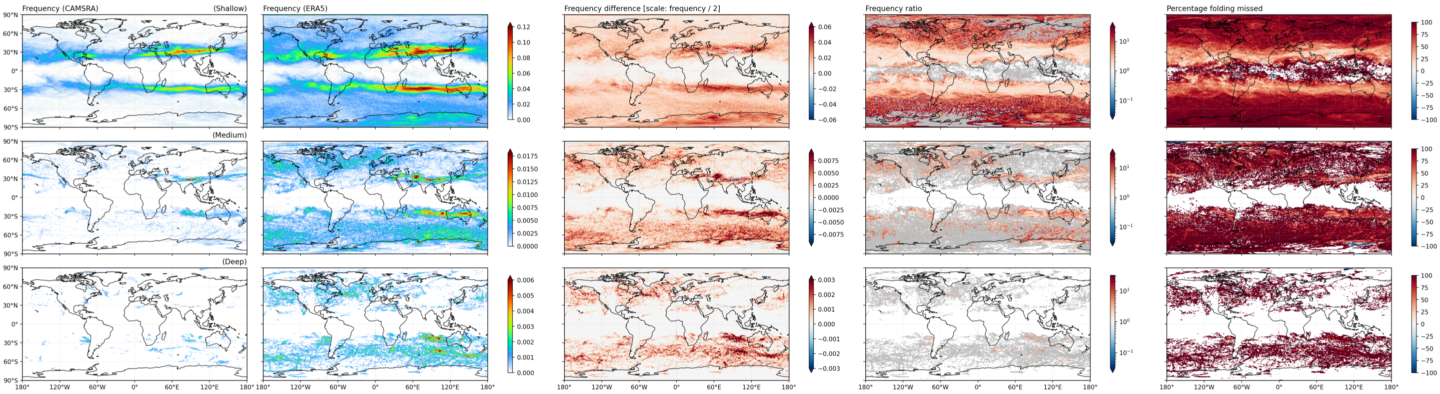

Figure S6. Folding frequency comparison by depth of folding. ***Top:*** (from left to right) Frequency of Shallow folding in CAMSRA and ERA5, their difference (ERA5–CAMSRA), their frequency ratio (ERA5/CAMSRA, with gray indicating zero denominator and non-zero numerator), and the percentage of folding in the higher-frequency of the two datasets that is missed by the lower-frequency of the two, as described in Figure S4's caption. ***Middle and bottom:*** As in top row but for Medium and Deep folding. Colorbar scales for the left three columns change across rows; those for the right two columns do not.

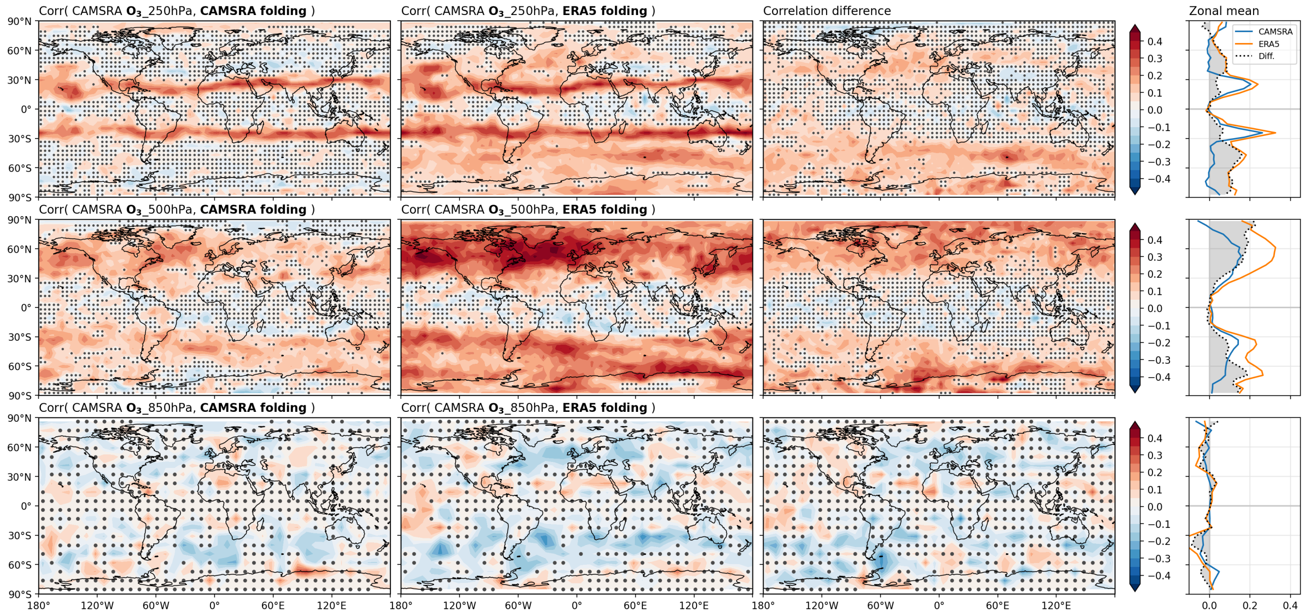

Figure S7. Correlations between CAMSRA tropospheric ozone and folding. As in Figure 3 but using total ozone O_3 instead of the stratospheric ozone tracer O_3S. The same conclusions are supported except at 850 hPa, where many other sources for tropospheric ozone besides the stratosphere are important. The correspondence of these maps at 250 and 500 hPa with those in Figure 3 indicates that O_3S is tightly related to total ozone at those levels.

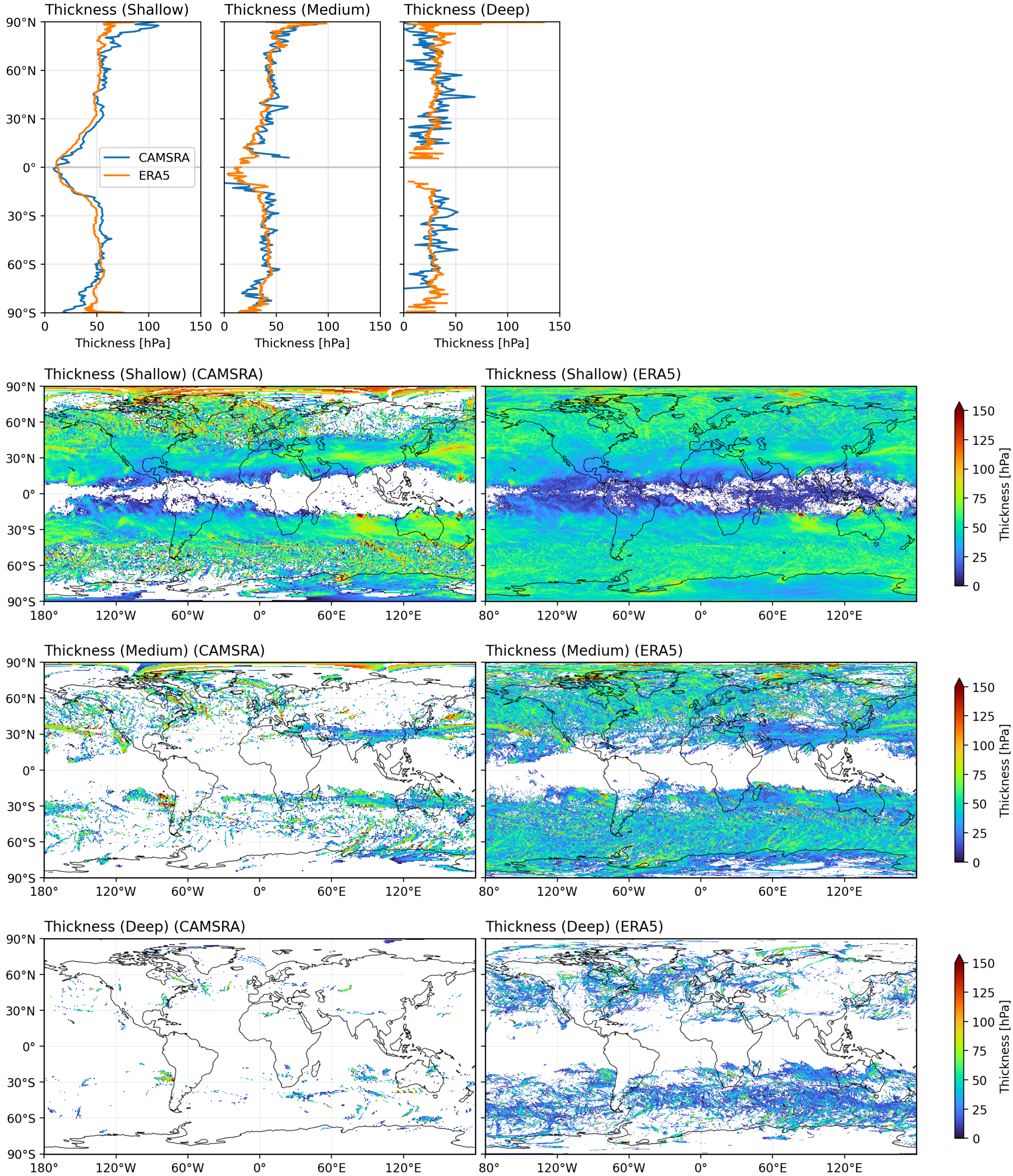

Figure S8. Thickness of folding in spatial detail. As in Figure S5 but for folding thickness (calculated as $pmax - (dp + pmin)$)

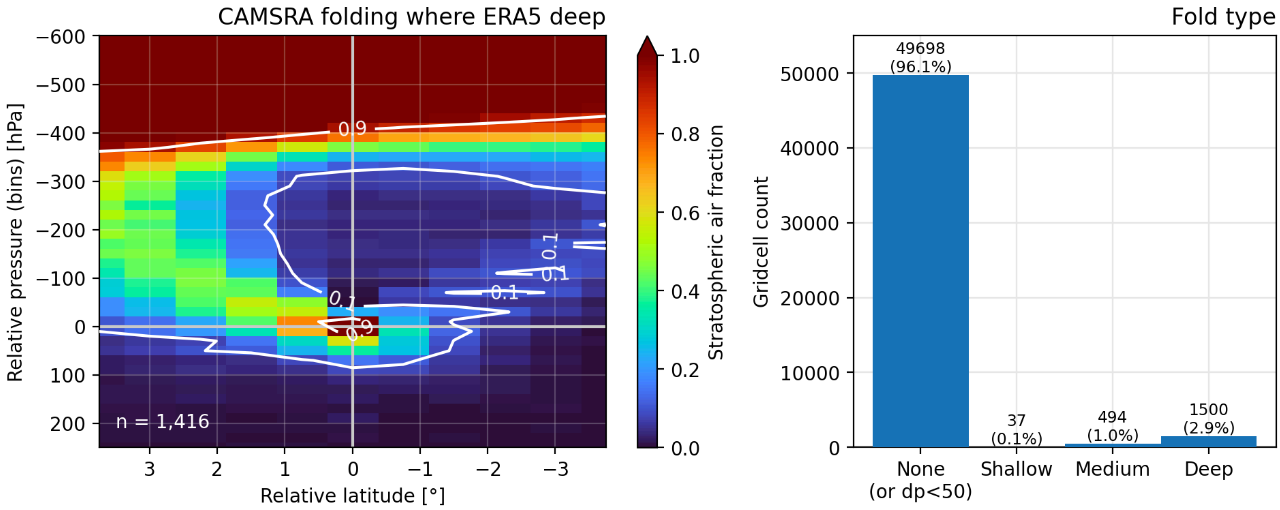

Figure S9. Fold cross-sections and folding types in CAMSRA where ERA5 identifies Deep folding. ***Left:*** A composite (as in Figure 4a–b) across 1,416 latitudinal cross-sections through column ranges in which any type of folding (Shallow, Medium, or Deep) is identified in CAMSRA at the same location and time that Deep folding is identified in ERA5. The 0.9 contour falls around 400 hPa above the top of the intrusion, which is closer than in ERA5 for all ERA5 Deep folding cases (Figure 4b). However, the 0.5 contour (not explicitly shown) is slightly over 350 hPa above, implying that for most of the cases in which CAMSRA does identify folding of any type, that folding is Deep. ***Right:*** Histogram of folding (or non-folding) types identified in all CAMSRA columns corresponding to Deep folding instances in ERA5. When folding is identified in CAMSRA it is most often Deep (1,500 columns) rather than Medium or Shallow (494 or 37 columns), in agreement with the cross-section composite (left [wherein all 2,031 of these columns belong to 1,416 contiguous latitudinal ranges]). However, across all 51,729 such columns, nearly all (96.1%) identify no folding at all in CAMSRA. Together these findings imply that CAMSRA is failing to resolve the tip of folds rather than resolving a fold at the wrong depth.